energies

MDPI

Article

Fast and Robust Hybrid Starter and Generator Speed Control for Improving Drivability of Parallel Hybrid Electric Vehicles

ByungHoon Yang [1], KyoungJoo Kim [1] and HyungSoo Mok [2,*]

[1] Research and Development Division, Hyundai Motor Company, 150, Hyundaiyeonguso-ro, Namyang-eup, Hwaseong-si, Gyeonggi-do 18280, Korea; ybh6679@hyundai.com (B.Y.); KJooKim@hyundai.com (K.K.)

[2] Department of Electronic Engineering, Konkuk University, 120 Neungdong-ro, Gwangjin-gu, Seoul 05029, Korea

* Correspondence: hsmok@konkuk.ac.kr

Received: 14 August 2020; Accepted: 21 September 2020; Published: 25 September 2020

Abstract: Speed control algorithms were studied to improve vehicle fuel economy and driving performance by rapidly combining two power sources—the engine and the driving motor. A hybrid starter and generator (HSG) was used in parallel hybrid vehicles, improving vehicle drive system efficiency by eliminating torque converters. The proposed zero-overshoot and zero-phase-error speed controller with active damping has the following three characteristics. First, it has an active damping structure resistant to load fluctuations (e.g., cranking torque fluctuation during engine starting). Second, there is no speed overshoot for the step command corresponding to the minimum engine running speed. Finally, it has no steady-state error for the ramp command generated by the moving vehicle. These control features reduce the time required to match the speeds of the two power sources, reducing delay when the vehicle starts and reducing energy consumption by minimizing unnecessary engine rotation. Simulation and vehicle test results proved that the proposed algorithm produced faster response characteristics and smaller steady-state errors than conventional control algorithms such as proportional-integral, integral-proportional, and two-degree-of-freedom algorithms. In this study, the fuel efficiency and driving performance of the hybrid vehicle could be improved by improving the performance of the speed control alone without any additional hardware changes.

Keywords: speed control; engine clutch; hybrid starter and generator; PI control; IP control; 2-DOF control; active damping; parallel hybrid vehicle; zero overshoot; zero phase error

1. Introduction

Recently, automobile manufacturers have been responding to regulations in individual countries by improving the fuel efficiency of existing vehicles or developing new vehicles that use alternative energy as a response to global warming and increased greenhouse gas emissions. As part of this response, various eco-friendly vehicles such as hybrid electric vehicles (HEVs), plug-in hybrid electric vehicles (PHEVs), electric vehicles (EVs), and fuel cell electric vehicles (FCEVs) have been developed. HEVs in particular, are generally classified into serial hybrid, parallel hybrid, and serial–parallel hybrid structures [1].

In particular, among the parallel hybrid systems, the transmission mounted electric device (TMED) system can only be operated with a driving motor having a relatively small power capacity at high speeds compared with that in series–parallel hybrid systems. Consequently, the power of the engine and the driving motor is delivered in parallel through fixed gear ratios without power circulation, offering good fuel economy and low construction costs [2].

However, if the driver's demand power surpasses the small power output of the driving motor, the engine's clutch is engaged after synchronizing the engine speed with the driving motor in order to use the engine power. A control system that synchronizes the engine speed and the driving motor speed as quickly and accurately as possible using a hybrid starter and generator (HSG) motor (connected to the engine with a belt) is required to ensure the vehicle's driving performance and minimize the energy used to rotate the engine. This speed control should respond rapidly to commands, be resilient to load changes caused by the engine start-up torque, and be resilient to parameter variations caused by various driving conditions, such as temperature and engine speed, to ensure the vehicle's drivability.

It is not easy to fully satisfy all of the above conditions with conventional linear control methods, such as proportional-integral (PI) control [3,4], integral-proportional (IP) control [4], and two-degree-of-freedom (2-DOF) control [5]. Moreover, adaptive control [6], robust control [7], slide mode control [8,9], disturbance observer based control [10], finite-time control [11], fractional order control [12], fuzzy control [13,14], neural network control [15,16], and many other control methods have been proposed to improve the speed control performance, each of which improves it in various ways. However, these control methods have complicated control structures, require large computational resources, and are not easy to design for a desired control bandwidth. The speed control method proposed herein is differentiated and contributes as follows:

(1) When the step speed command is applied, speed overshoot and steady-state errors scarcely occur. Since the speed command tracking performance is similar to that of a first-order low-pass filter (LPF), the proposed controller can be designed by predicting the control performance using the time constant concept when designing the control performance.
(2) When the ramp speed command is applied, it results in a very small steady-state error. Since forward compensation for the command is used, it does not react to speed measurement noise applied through the feedback loop of the speed controller. The forward compensator is based on an inverse function of the speed controller; therefore, the gain design of the forward compensator is simple.
(3) The proposed speed control method is resilient to parameter variations, such as the moment of inertia and the viscous friction coefficient required for controller design. Even if parameter variation occurs, the effect on the designed control bandwidth is small, and the steady-state error for step or ramp commands is small.
(4) The variation in speed is small as the proposed method uses a structure that increases the damping of the entire system using the speed for feedback even if an uncertain disturbance is encountered.
(5) A method of designing the controller gain considering the constraints of the system is presented. When limiting the rate of change of torque to prevent belt slip in order to guarantee the durability of the system (connected by belt), a method for designing a control gain considering the rate of change of torque and disturbance type is presented.

In this study, we compare and validate the aforementioned characteristics of the proposed method through simulation and vehicle testing with linear controllers of a similar form used in the conventional speed control methods.

2. Preliminaries

This section describes the schematic features of the TMED system and the mathematical model of the target system.

2.1. Outline and Features of TMED Systems

The mechanical configuration of the TMED system is shown in Figure 1.

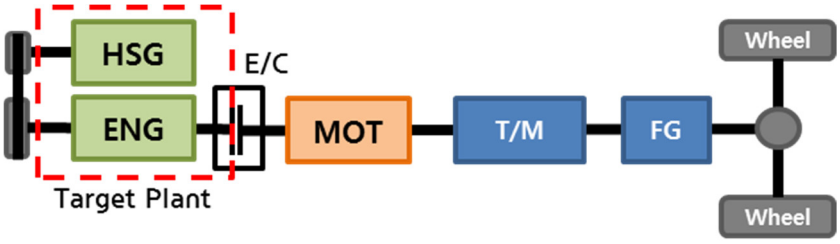

Figure 1. TMED system structure.

In Figure 1, the HSG serves to start the engine or charge the main battery, ENG is a gasoline engine, E/C is an engine clutch, MOT is a driving motor, T/M is a six-speed automatic transmission, FG is the final reduction gear, and Wheel is the driving wheel. Herein, the object to be controlled is the HSG, which is integrated with the ENG and belt system as shown in Figure 2.

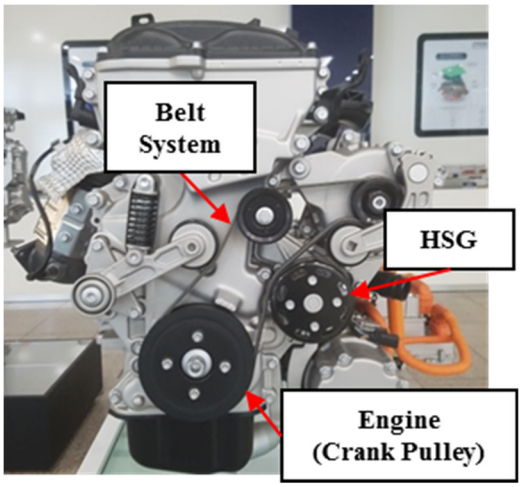

Figure 2. Engine–HSG construction combined with the belt system.

The TMED system has a structure that eliminates the torque converter to improve fuel efficiency. Owing to these features, when the vehicle starts to move, it uses the driving motor to start driving and then starts the engine, engaging the engine clutch between the engine and the motor to use the two combined power sources. The profile of speed command and load torque for starting after stopping is shown in Figure 3.

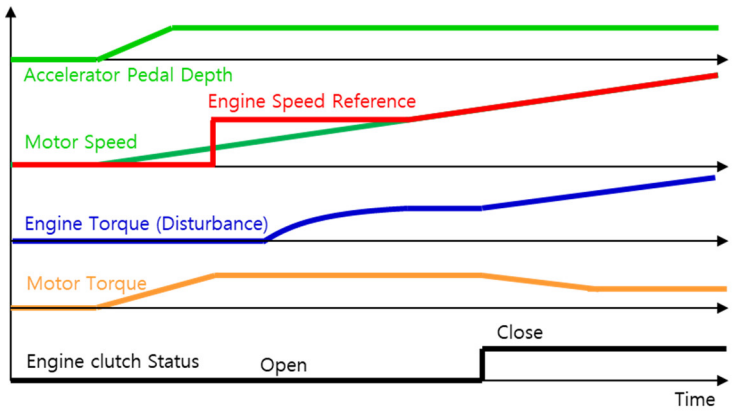

Figure 3. Speed command/load torque profile for vehicle launch of the TMED system.

2.2. Mathematical Model of HSG

The HSG mechanical system has the structure shown in Figure 2. If the tension of the belt system is high enough and belt slip does not occur, the HSG and engine can be modeled as an integrated system as shown in Figure 4.

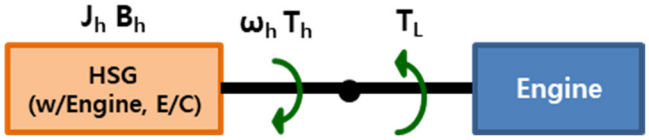

Figure 4. Simplified HSG system model.

J_h and B_h in Figure 4 indicate the moment of inertia and coefficient of viscous friction of the entire system observed on the HSG side, respectively [17].

The simplified system transfer function shown in Figure 4 can be expressed as the following equation:

$$T_h = J_h \frac{d\omega_h}{dt} + B_h\omega_h + T_L \tag{1}$$

$$\omega_h = \frac{1}{J_h}\int (T_h - T_L - B_h\omega_h)dt \tag{2}$$

$$G_p(s) = \frac{1}{J_h s + B_h} \tag{3}$$

where T_h, J_h, B_h, ω_h, T_L, and $G_p(s)$ represent the output torque of the HSG, the moment of inertia of the HSG system, the viscous friction coefficient of the HSG system, the rotational angular speed of the HSG, the load torque by engine, and transfer function of the control target, respectively. Since the viscous coefficient of friction of the engine may vary depending on the temperature of the engine oil used for cooling or the speed at which it is rotating, it may affect the entire system viscous friction coefficient B_h observed on the HSG side [18]. Figure 5 shows the friction characteristics according to engine speed and oil temperature.

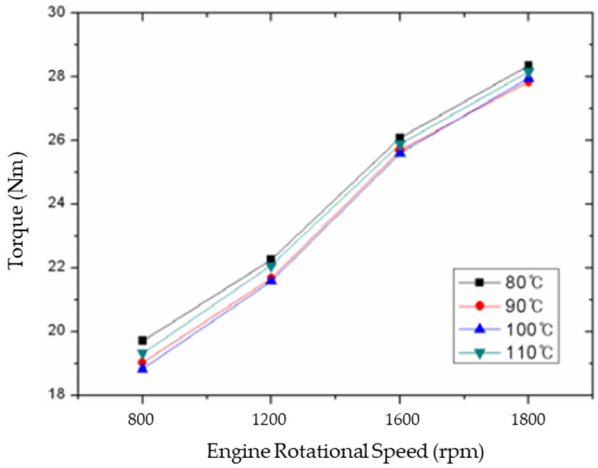

Figure 5. Friction characteristics according to engine rotational speed and engine oil temperature.

The moment of inertia of the HSG system does not vary significantly with the environment. Therefore, it can be estimated by outputting a constant torque and observing the speed change of the HSG. In this work, the mechanical parameters used for control, i.e., the moment of inertia and the coefficient of friction, are estimated using the mechanical equation under the assumption that torque output and speed of the HSG can be measured. The friction characteristics shown in Figure 5 mainly

vary with the engine rotational speed. Therefore, the estimated friction coefficient for the HSG system can be obtained by using the following equation for each speed:

$$\hat{B}_h = \frac{T_h}{\omega_h} \tag{4}$$

where $\hat{B}_h$ is the estimated friction coefficient for HSG systems. The inertia of the system is estimated using the variation in the average speed measured during the application of specific torque as well as acceleration and deceleration of the HSG [19]:

$$\hat{J}_h = \frac{T_h - B_h \cdot \omega_h}{\frac{d\omega_h}{dt}} \tag{5}$$

where $\hat{J}_h$ and $\frac{d\omega_h}{dt}$ represent the value of the estimated moment of inertia of the HSG system and the differential value of the HSG rotational speed, respectively. Figure 6 shows the estimated $\hat{B}_h$ when releasing the engine clutch with the vehicle stopped and increasing the HSG speed from 2000 rpm to 5000 rpm. The HSG rotational speed is 1/2.5 times the engine rotational speed according to the pulley ratio. In the case of the hybrid vehicles considered in this study, the minimum starting speed of the engine is approximately 1000 rpm, and if the engine is started while driving, the engine speed could be less than 2000 rpm. Therefore, considering the pulley ratio, the HSG speed range for estimating $\hat{B}_h$ was estimated by selecting the range from approximately 2500 rpm to 5000 rpm. The expression of the units is based on $\hat{B}_h$ as estimated at 2500 rpm.

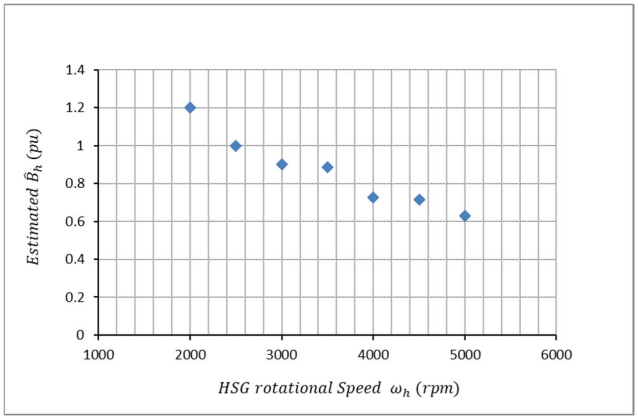

Figure 6. Estimated viscous friction coefficients according to the HSG speed.

In addition, a block diagram of the HSG inverter system is as shown in Figure 7. The speed controller generates HSG output torque command T_h^* so that ω_h follows ω_h^* by feeding back HSG speed ω_h after receiving the speed command ω_h^* from the host controller. The HSG current command is converted by using the torque constant K_t to follow the HSG torque command, which is the output of the speed controller. To generate the command torque, the inverter system feeds back the phase currents of the HSG motor to perform current control and uses the DC-link voltage of the inverter to generate the average output voltage with the insulated gate bipolar transistor (IGBT) switch to perform current control. If the output voltage generation period is more than ten times larger than the control bandwidth of the current controller and the current controller bandwidth is ten times larger than the speed controller bandwidth, the output gain of the entire system for generating torque can be approximated as 'unity' [20].

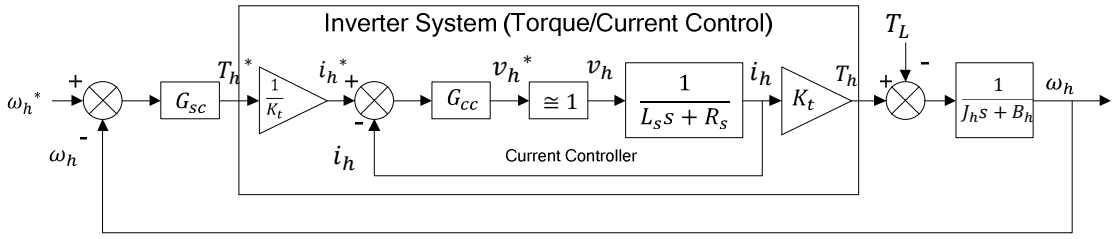

Figure 7. The HSG system control block diagram.

The transfer function of the output torque of the above HSG system is as follows:

$$\frac{T_h(s)}{T_h{}^*(s)} = \frac{i_h(s)}{i_h{}^*(s)} = \frac{\omega_{cc}}{s + \omega_{cc}} \cong 1 \tag{6}$$

where $T_h(s)$, $T_h{}^*(s)$, $i_h(s)$, $i_h{}^*(s)$, and ω_{cc} represent the HSG output torque, the HSG output torque command, the HSG output current, the HSG output current command, and current controller bandwidth, respectively.

3. Design of Speed Controller

3.1. Conventional Speed Controllers

In conventional speed controllers, aspects such as the proportional gain and integral gain of the controller were selected using a model that simplified the system by including the friction coefficient B_h, a system parameter, in the load torque T_L.

If the above simplified model is used in the conventional PI speed controller, the first and zero order coefficients of the numerator of the transfer function are the same as the first and zero order of the coefficients of the denominator. Therefore, it is difficult to apply the general method of selecting the gain by making the response characteristic of the control system equal to the first delay factor by designing the zero point of the proportional integral controller to cancel the pole point of the system. The most popular method is the "approximate gain selection method" [3]. The response characteristic of the controller is selected by designing the control bandwidth ω_{sc}. This was set to −3 dB in the frequency band where the transfer function of speed/speed command was designed. In systems with transfer functions such as those listed in Table 1, when a step speed command is applied, an overshoot of speed occurs owing to the effect of the zero in the numerator. This response characteristic increases the time taken for the control target to reach the target speed, thereby increasing the duration for which the engine clutch is engaged.

Table 1. Transfer function of each controller.

Controller	PI	IP	2-DOF	Proposed
$\frac{\omega_h(s)}{\omega_h{}^*(s)}$	$\frac{K_p s + K_i}{J_h s^2 + (B_h + K_p)s + K_i}$	$\frac{K_i}{J_h s^2 + (B_h + K_p)s + K_i} = \frac{{\omega_n}^2}{s^2 + 2\zeta\omega_n s + {\omega_n}^2}$	$\frac{aK_p s + K_i}{J_h s^2 + (B_h + K_p)s + K_i}$	$\frac{(K_p s + K_i)(s + \omega_{sc})}{\{J_h s^2 + (B_h + B_a + K_p)s + K_i\}\omega_{sc}} = 1$
$\frac{\omega_h(s)}{T_L(s)}$	$\frac{-s}{J_h s^2 + (B_h + K_p)s + K_i}$	$\frac{-s}{J_h s^2 + (B_h + K_p)s + K_i}$	$\frac{-s}{J_h s^2 + (B_h + K_p)s + K_i}$	$\frac{-s}{J_h s^2 + (B_h + B_a + K_p)s + K_i}$

In the case of the IP controller, the control gain was selected so that the system transfer function was in the form of a second LPF, assuming a simple system that included the friction coefficient in the load torque. In the IP controller transfer function listed in Table 1, and ω_n represent the damping ratio and natural frequency, respectively [4]. For a fair comparison with other controllers, the control bandwidth of the IP controller, ω_n, was selected so that the magnitude of the transfer function output of the speed/speed command was −3 dB, giving it similar response characteristics to other controllers

with the control bandwidth of ω_{sc}. Here, as shown in Table 2 below, when the damping coefficient is changed, the K_p and K_i gains also change. However, the K_i gain changes excessively according to the design variation of the damping ratio, and in order to increase the damping ratio, a suitable anti-windup controller is required to prevent over-integration of the integrator. In addition, applying the final value theorem for the ramp instruction using a transfer function to predict the magnitude of the steady-state error, it can be observed that the IP controller had a larger steady-state error than the PI controller. Owing to such a response characteristic, the speed difference between the motor and the engine was so large that the engine clutch could not be engaged, or if the engine clutch is forcibly engaged when the speed difference between the two power sources is large, the feeling of acceleration or deceleration could be felt from the side of the vehicle.

Table 2. Gain comparison between controllers (at ω_{sc} = design value).

Controller	PI	IP	2-DOF	Proposed
ω_n	-	$\frac{\omega_{sc}}{\sqrt{1-2\zeta^2+\sqrt{2-4\zeta^2+4\zeta^4}}}$	$\frac{\omega_{sc}}{\sqrt{1-2\zeta^2+\sqrt{2-4\zeta^2+4\zeta^4}}}$	-
K_p	$\hat{J}_h \times \omega_{sc}$	$2\zeta\omega_n\hat{J}_h$	$2\zeta\omega_n\hat{J}_h$	$\hat{J}_h \times \omega_{sc}$
K_i	$K_p \times \frac{\omega_{sc}}{5}$	$\hat{J}_h{\omega_n}^2$	$\hat{J}_h{\omega_n}^2$	$\left(\hat{B}_h + B_a\right) \times \omega_{sc}$
α	-	-	0.5	-
B_a	-	-	-	Multiple of $\hat{B}_h$

The 2-DOF controller has intermediate characteristics between those of the PI and IP controllers based on the value of ''. As with the other controllers, B_h is considered to be included in the load torque for controller gain selection, and the system is simplified and analyzed accordingly. The 2-DOF controller has the same characteristics as those of the IP controller when the '' value is 0, and the same characteristics as those of the PI controller when the '' value is 1 [5]. Here, K_p and K_i control gains were selected so that the load response characteristics had the same performance as that of the IP controller. The response characteristics were then compared with those of other controllers. Designing with an '' value of 0.5 results in intermediate characteristics between those of the IP controller and PI controller. However, if the control gain is designed so that the load response characteristics are identical to those of the IP controller, proper anti-windup control is required as the integration gain becomes excessively large. In addition, since the steady-state error characteristic of the 2-DOF controller's ramp command has an intermediate response characteristic between those of the PI controller and the IP controller, the disadvantage of the IP controller (i.e., significant steady-state error) may appear.

3.2. Proposed Speed Controller

The proposed speed controller in this work has the following features.

First, the controller gain was selected using a system model that reflected the friction coefficient, unlike the existing controller, which was simplified without including the friction coefficient in the transfer function of the target. The selected controller's gain was able to suppress the speed overshoot by canceling the zero of the numerator of the transfer function for the speed/speed command.

Second, by applying an active damping structure and designing a control gain that reflects the damping structure in the feedback controller, it is possible to independently design the characteristics of load fluctuations. Such a structure may have a larger integral gain than conventional controllers, but owing to the role of its active damping controller that uses speed feedback, the output value accumulated in the integrator is small, making it easy to design an anti-windup controller.

Third, the proposed speed controller has a structure that compensates for the speed command using the designed control bandwidth, so it is easy to select the forward compensation control gain and eliminate the steady-state error as there is no phase delay, even when the ramp command is applied. The proposed controller has a structure in which a command forward compensator (which compensates for the change of the command) and a feedback controller (which follows the compensated speed

command), are connected in series. In this discrete control structure, when a step command is applied, the magnitude of the command during one control cycle at the point at which the command changes can be increased by multiplying the reciprocal of the controller's operating cycle by the difference between the previous speed command value and the current speed command value. However, when a steady-state without command change is reached, the output of the command compensator becomes the same as that of the command and shows the response characteristic of the feedback controller only.

In discrete control, the magnitude of the torque output during one sample period can be very large, but the effect on the actual controller is small, owing to output limitations such as current control bandwidth and torque output rate limitation. Therefore, it can be said that the response to the step command has the characteristics of the transfer function, as shown in Equation (7):

$$\frac{\omega_h(s)}{\omega_h{}^*(s)} = \frac{K_p s + K_i}{J_h s^2 + (B_h + B_a + K_p)s + K_i} \tag{7}$$

where B_a is an active damping coefficient for increasing damping of the control system. In addition, in the case of the ramp command, if the command forward compensator is designed to compensate for the phase delay of the feedback controller, Equation (8) becomes a 'unity' function, and no steady-state error occurs.

$$\frac{\omega_h(s)}{\omega_h{}^*(s)} = \frac{(s + \omega_{sc})}{\omega_{sc}} \frac{K_p s + K_i}{J_h s^2 + (B_h + B_a + K_p)s + K_i} \tag{8}$$

To select a control gain that satisfies the response characteristics of the step command, the control gain can be designed using the transfer function of Equation (7), excluding the forward compensation term. Selection of a control gain to design the entire transfer function in the form of a controller ($\frac{1}{\tau s+1}$) of the 1st LPF structure with constant performance without overshoot is as shown in Equations (9) to (14).

This characteristic makes it easy to predict the time constant reaching a steady-state value using the control bandwidth. In Equation (7), the coefficients of the first and second terms are obtained so that the transfer function of the denominator is designed to cancel the zero of the numerator.

$$J_h s^2 + \left(K_p + B_h + B_a\right)s + K_i = \left(K_p s + K_i\right)(\tau s + 1) \tag{9}$$

$$J_h s^2 + \left(K_p + B_h + B_a\right)s + K_i = \tau K_p s^2 + \left(K_p + \tau K_i\right)s + K_i \tag{10}$$

$$K_p = \hat{J}_h \times \omega_{sc} \left(\because \tau = \frac{1}{\omega_{sc}}\right) \tag{11}$$

$$K_p + B_h + B_a = K_p + \tau K_i \tag{12}$$

$$\tau K_i = B_h + B_a \tag{13}$$

$$K_i = \left(\hat{B}_h + B_a\right) \times \omega_{sc} \left(\because \tau = \frac{1}{\omega_{sc}}\right) \tag{14}$$

To predict the load response characteristics, the transfer function of ω_h for T_L is obtained based on the proposed controller in Figure 8, as expressed by Equation (15).

$$\frac{\omega_h(s)}{T_L(s)} = \frac{-s}{J_h s^2 + \left(B_h + B_a + K_p\right)s + K_i} \tag{15}$$

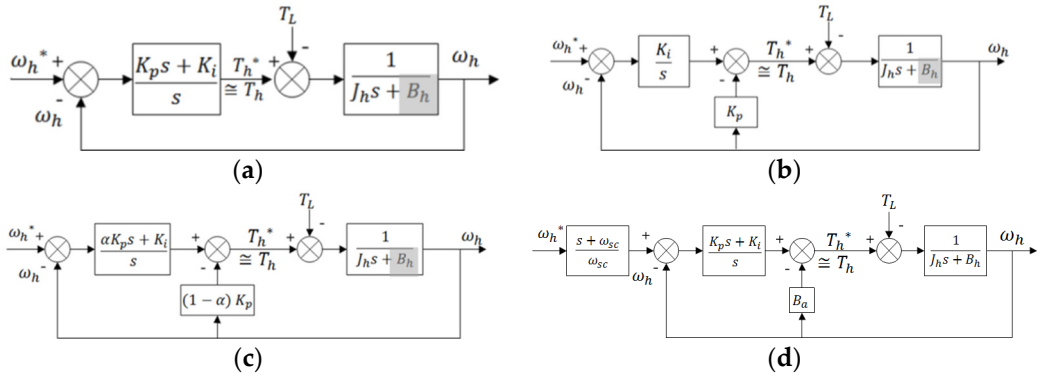

Figure 8. Block diagram of each controller. (**a**) PI controller, (**b**) IP controller, (**c**) 2-DOF controller, and (**d**) Proposed controller.

By designing B_a to improve the load response characteristics, it is possible to change the influence of ω_h variation on T_L. The control block diagram, transfer function, and control gain formula for each controller are shown in Figure 8, Tables 1 and 2, respectively.

3.3. Design of the Proposed Controller Gain

The proposed controller can regulate the response characteristics by selecting the control bandwidth of the speed controller and the magnitude of the damping coefficient of the active damping controller.

(1) In the entire control system, if the current (torque) controller control bandwidth of the inner loop is more than ten times greater than that of the outer loop speed controller, the output of the current controller has a very small effect on the speed controller and can be ignored. If the control bandwidth of the current controller operating in the inner loop is 200 Hz, the control bandwidth of the speed controller operating in the outer loop must satisfy the condition of 20 Hz or less. However, since the 1st LPF with a cut-off frequency of 20 Hz is used to block noise at the HSG speeds used as the speed controller inputs, the control bandwidth was designed to be less than 1/5 of the filter cut-off frequency to minimize the effect of the filter. Considering all the above, the control bandwidth of the speed controller can be selected to be 4 Hz or less—herein, it was designed to be 3 Hz, to simulate and test the vehicle.

(2) The control gain of the active damping controller should be designed in consideration of the limitations on the output torque of the HSG (maximum output, maximum torque, output torque change rate, etc.) and the output characteristics of the engine operating under load. The characteristics to be considered in particular are the constraints limiting the change rate of HSG output torque to prevent belt slip occurrence and the magnitude of HSG speed variation owing to C2 oscillations having twice the frequency of engine rotation produced by the operating characteristics of the engine. The time constant of the mechanical system represented by Equation (16) can be determined using the designed active damping coefficient.

$$\hat{G}_p(s) = \frac{1}{J_h s + B_h + B_a} \tag{16}$$

where $\hat{G}_p(s)$ is the transfer function of the plant for which active damping control is considered. It is necessary to design the machine time constant within a specific value to satisfy the abovementioned constraints and to operate the entire speed controller in the linear region. When the time constant value of the mechanical system satisfies this condition, it is easy to design an anti-windup controller as the difference between the output torque of the controller and the actual output torque is sufficiently small. The magnitude of the C2 vibration produced by the engine characteristics was experimentally measured as ±10 Nm, and the maximum rate of change of the output torque of the HSG system used in this study is 8 Nm/10 ms. If the load torque waveform is sinusoidal, then the frequency of the

maximum output torque can be obtained by differentiating the sine wave. Therefore, an operable frequency of 12.732 Hz can be obtained based on the value of 800 Nm/s, which is the amount of change in the maximum output torque. The value of B_a that can be designed to attenuate the above load fluctuation without distortion of the torque waveform is expressed in Equation (17):

$$\frac{B_h + B_a}{J_h} \leq \omega_{load\_MAX} \tag{17}$$

$$B_a \leq \omega_{load_{MAX}} \times J_h - B_h \tag{18}$$

where $\omega_{load_{MAX}}$ is the maximum frequency applied to the load torque. Herein, the value of B_a can be designed in a range that satisfies Equation (18) [21,22]. Table 3 lists the control gain values used in the simulation to compare the characteristics of each controller.

Table 3. Simulation controller gain (at ω_{sc} = 18.85 rad/s).

Controller	PI	IP	2 DOF	Proposed
K_p	0.622	1.933	1.933	0.622
K_i	2.345	28.307	28.307	49.536
α	-	-	0.5	-
B_a	-	-	-	2.603

4. Simulation Results

The step/ramp command response characteristics of each controller listed in Table 1 can be predicted using the steady-state error of each controller by applying the final value theorem using the parameters applied to the simulation. Table 4 shows the steady-state error for each command for the speed/speed command transfer function of each controller. If the design parameters are correct, it can be expected that the proposed controller would not cause a steady-state error.

Table 4. Steady-state error for each controller (at A = 3000 rpm/s).

Controller	PI	IP	2-DOF	Proposed
Final value theorem of ramp command: $\lim_{s\to 0} \frac{A}{s^2}\left(1 - \frac{\omega_h(s)}{\omega_h{}^*(s)}\right)$	$\frac{AB_h}{K_i}$	$\frac{A\left(B_h+K_p\right)}{K_i}$	$\frac{A\left(B_h+K_p-\alpha K_p\right)}{K_i}$	$\frac{(B_h+B_a)\omega_{sc}-K_i}{K_i\omega_{sc}}$
Ramp command error (rpm)	Δ46.05	Δ208.68	Δ106.24	0

4.1. Frequency Domain Analysis

If the magnitude of the response in the Bode diagram for speed/speed command does not exceed 0 dB, even if the entire frequency range command is applied, the speed does not exceed the command. As can be seen in Figure 9, the conventional PI controller has a frequency band whose response magnitude exceeds 0 dB owing to the zero in the numerator of the transfer function, so when the command in this frequency band is applied, the speed exceeding the magnitude of the command may occur. In the case of the IP controller, 2-DOF controller, and proposed controller, the overshoot of the feedback speed does not occur because the total area gain of the frequency response is less than 0 dB. In addition, even in the case of a speed response to load fluctuation, it can be expected that the speed fluctuation will be smallest when the load fluctuates because the gain of the proposed controller is always lower (in all frequency ranges) than those of the conventional controllers.

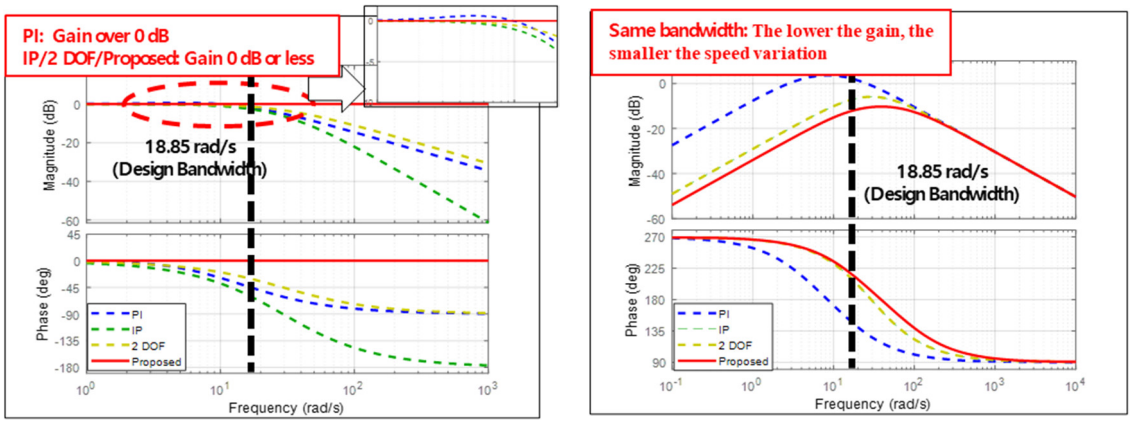

(**a**) (**b**)

Figure 9. Speed response for each controller (frequency domain). (**a**) Speed response to speed command, (**b**) Speed response to load torque.

4.2. Time Domain Analysis

To intuitively compare the analysis of Figure 9, which shows the speed response results for each controller in the frequency domain, Figure 10 shows the simulation results of the speed response in the time domain. In order to compare the control response according to the EV→HEV mode conversion profile under conditions similar to those of the actual vehicle, the response of the speed/speed command and the response to the speed/load torque in the time domain were estimated by considering the HSG specification.

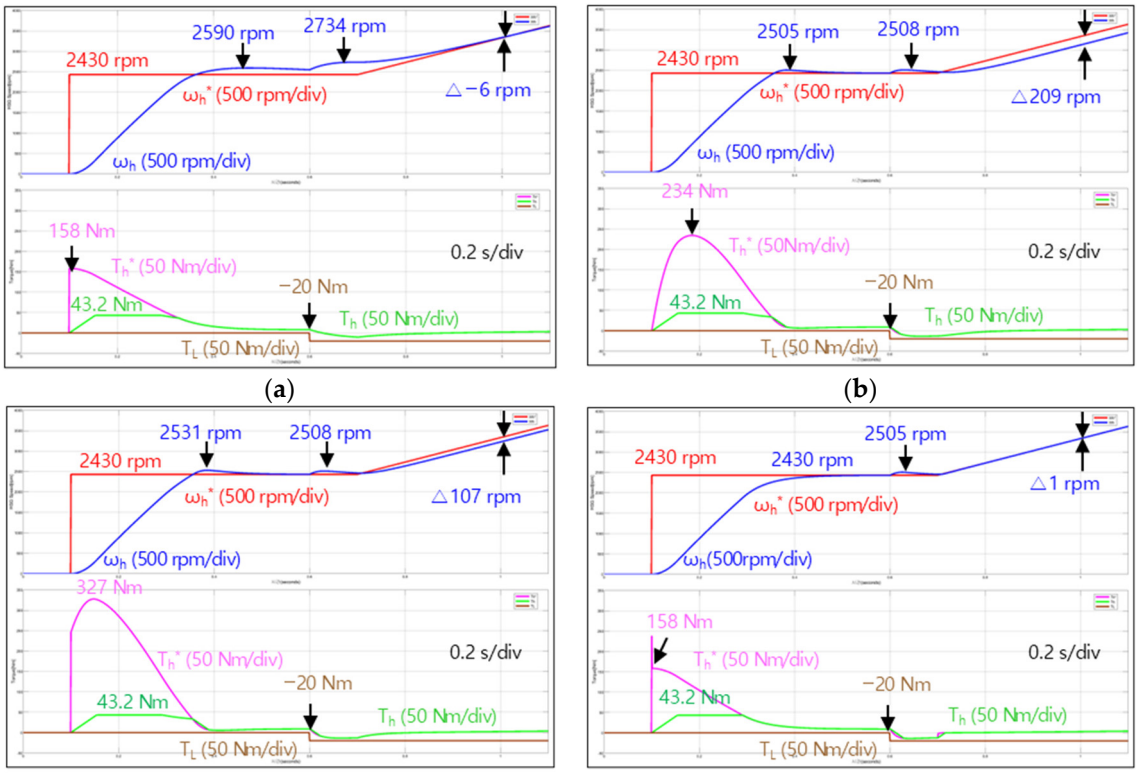

(**a**) (**b**)

(**c**) (**d**)

Figure 10. Simulation result when the speed command profile is applied (step: 2430 rpm, ramp: 3000 rpm/s, and load: −20 Nm). (**a**) PI controller, (**b**) IP controller, (**c**) 2-DOF controller, and (**d**) Proposed controller.

The conventional PI controller has poor speed-following characteristics for the step command owing to speed overshoot and a large speed variation owing to the load fluctuation. However, the steady-state error for the ramp command was predicted to be better than the expected result because the response characteristic with the applied load torque and the original steady-state error characteristic were added.

The conventional IP controller predicted that no overshoot would occur in the frequency domain, but a slight overshoot did occur owing to the excessive integral controller output. The response characteristics of the load fluctuation showed the same speed fluctuation as that of the 2-DOF controller; the steady-state error of the ramp command was greater than those of the other controllers.

The 2-DOF controller showed characteristics similar to those of the IP controller, but the steady-state error for the ramp command was smaller than that of the IP controller. The proposed controller was able to anticipate that the speed followability for a given profile would be superior to that of the other controllers. A comparison of the above simulation results is summarized in Table 5.

Table 5. Comparison of control characteristics for each controller (rpm).

Controller	PI	IP	2-DOF	Proposed
Speed overshoot	160	75	101	0
Speed variation at load disturbance	304	78	78	75
Steady-state error (At ramp command)	−6	209	107	1

4.3. Robustness Analysis

As in Section 2, the friction coefficient B_h among the system parameters varies depending on the rotational speed of the HSG. In addition, since the system inertia, J_h, may differ by vehicle, it is necessary to predict speed/speed command and speed/load torque for parameter fluctuations.

However, since it is difficult to prepare several test objects with different parameters, a simulation was performed by changing the parameters $\hat{J}_h$ and $\hat{B}_h$ used for gain calculation in the controller. In Figures 11 and 12, the response characteristics of the parameter variations for each controller are compared. The range of each parameter variation was compared by selecting 50–250% of the reference value.

Table 6 shows the steady-state error for each controller for the ramp command as the speed error. The proposed controller is predicted to have a very small steady-state error, even if parameter errors occur.

Table 6. Steady-state error by each controller [rpm] (at 3000 rpm/s ramp).

Controller	Parameters Variation		
	50%	100%	250%
PI	92.11	46.05	18.42
IP	212.49	208.68	206.39
2 DOF	110.06	106.24	103.95
Proposed	0.00072	0	−0.0043

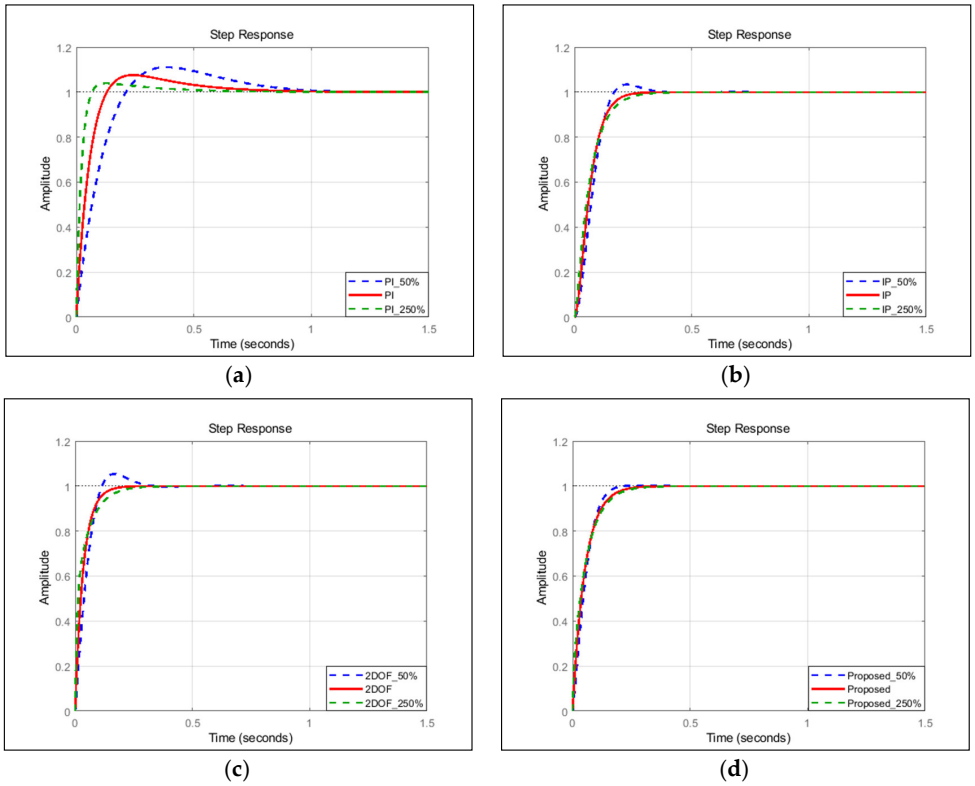

Figure 11. Speed/speed command response characteristic of each speed controller according to parameter variation (at 50%, 100%, and 250% variation of $\hat{J}_h$ and $\hat{B}_h$). (**a**) PI controller, (**b**) IP controller, (**c**) 2-DOF controller, and (**d**) Proposed controller.

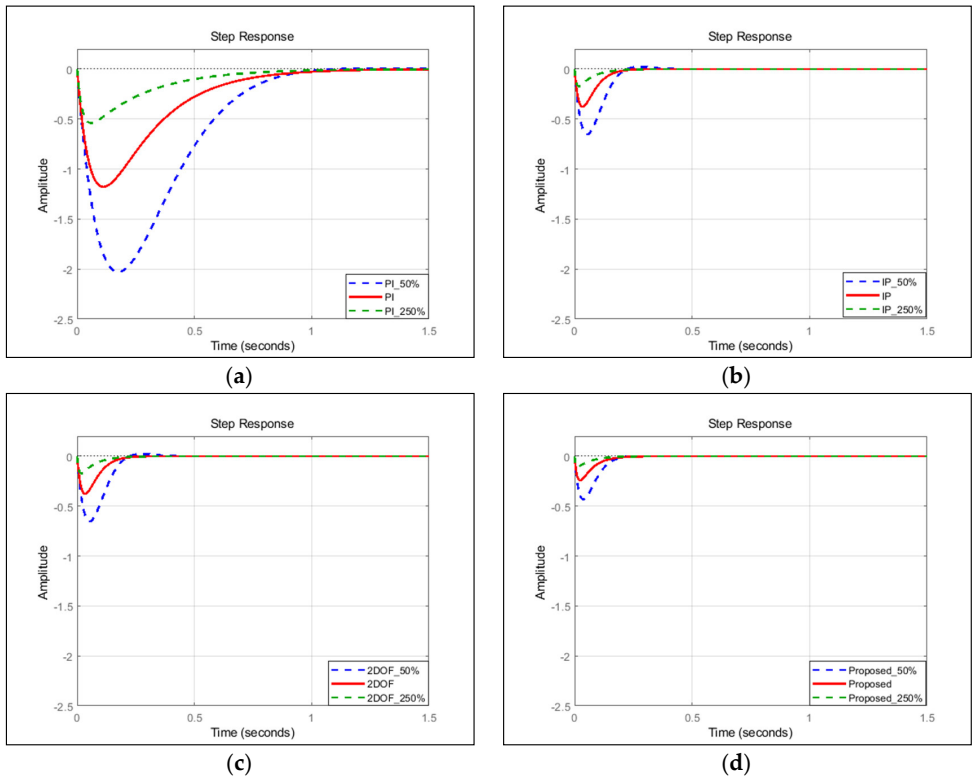

Figure 12. Speed/load torque response characteristics of each speed controller according to parameter variation (at 50%, 100%, and 250% variation of $\hat{J}_h$ and $\hat{B}_h$). (**a**) PI controller, (**b**) IP controller, (**c**) 2-DOF controller, (**d**) and Proposed controller.

5. Vehicle Test Results

A control performance test measured the response characteristics of the step command and ramp command with the engine clutch released during the vehicle's stopping, to confirm that the results predicted in the simulation were in fact obtained experimentally. Since the actual values of J_h and B_h may vary, as discussed in Section 2 earlier, it is necessary to use several samples to consider the effect of parameter variation.

However, since it is difficult to test several samples, the robustness against parameter fluctuation was confirmed by varying the parameters $\hat{J}_h$ and $\hat{B}_h$ used for controller gain to 50%, 100%, and 250%. The final verification test validated the proposed method by comparing the speed control execution time with those of other controllers, while keeping the accelerator pedal constant, to compare the effect of speed control on the driving performance of the vehicle when engaging the actual engine clutch.

5.1. Step Command Response

The result of the test wherein the step command was applied while the vehicle was stationary is shown in Figures 13–15. For the test conditions, commands of (1) 0 rpm, (2) 3000 rpm, and (3) 0 rpm were applied for each controller in the form of a step.

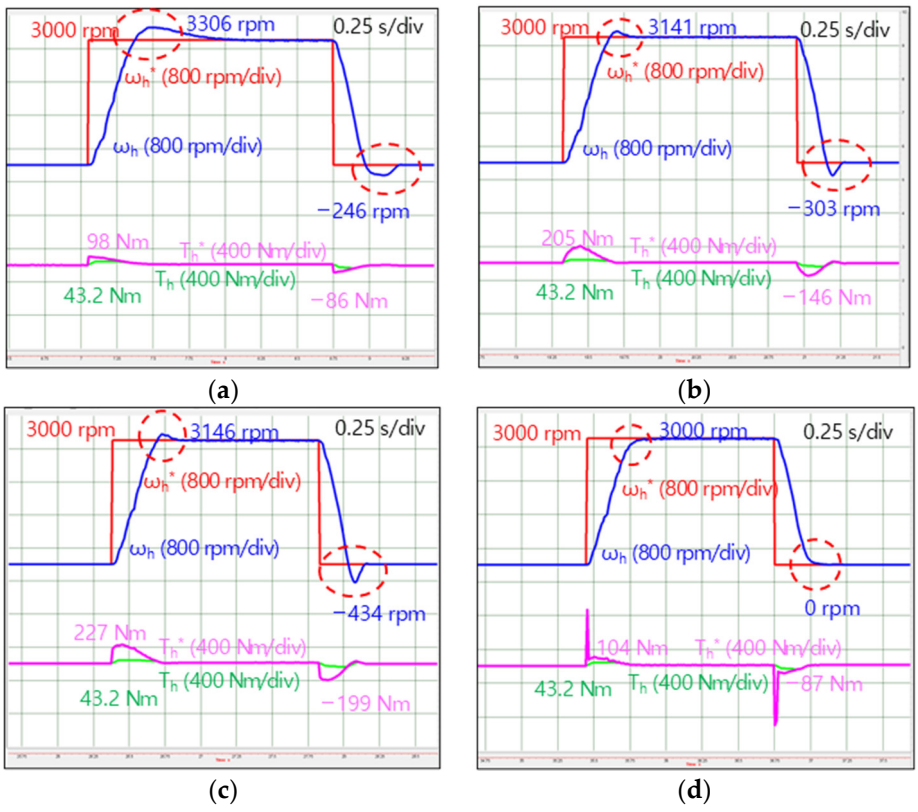

Figure 13. Speed control for step command (at 3000 rpm, parameters varied by 50%). (**a**) PI controller, (**b**) IP controller, (**c**) 2-DOF controller, and (**d**) Proposed controller.

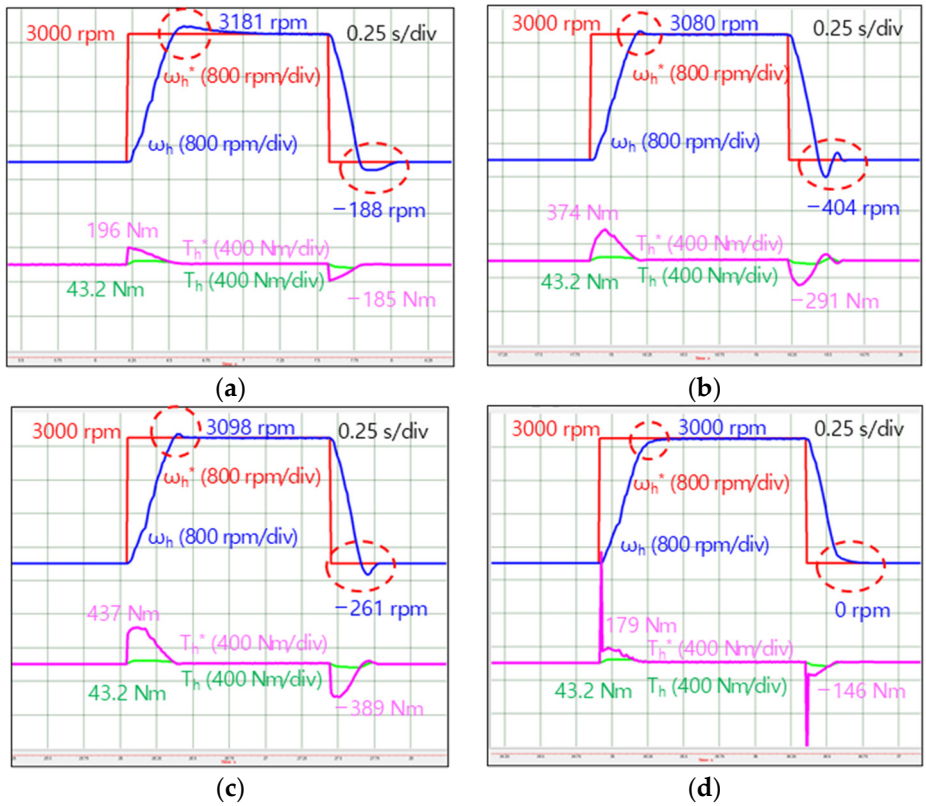

Figure 14. Speed control for step command (at 3000 rpm, parameters varied by 100%). (**a**) PI controller, (**b**) IP controller, (**c**) 2-DOF controller, and (**d**) proposed controller.

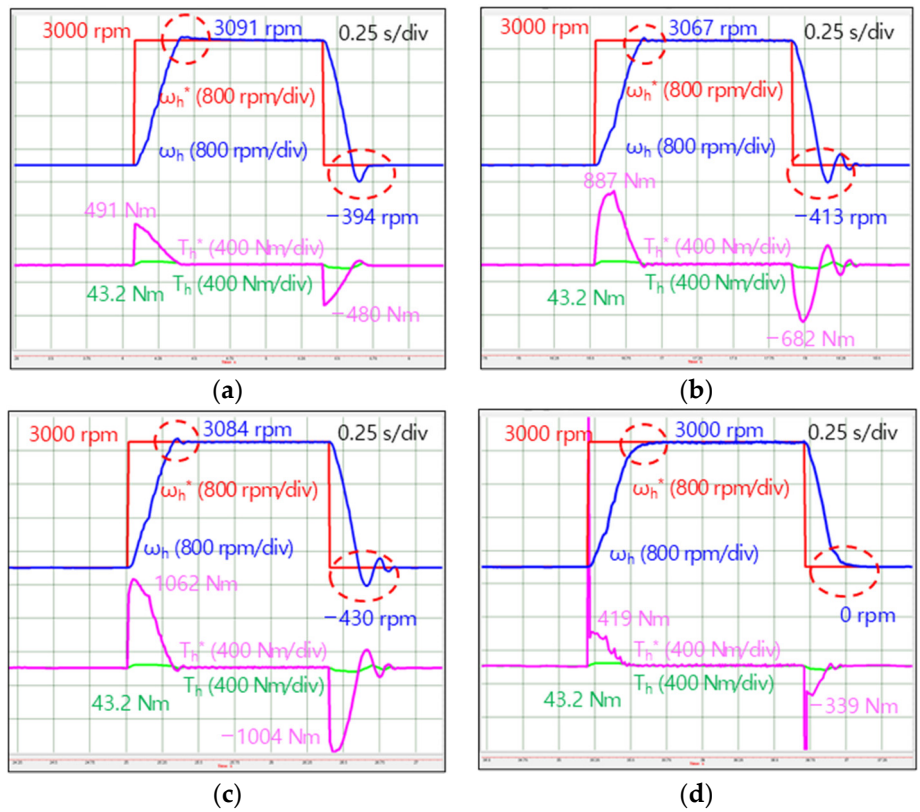

Figure 15. Speed control for step command (at 3000 rpm, parameters varied by 250%). (**a**) PI controller, (**b**) IP controller, (**c**) 2-DOF controller, and (**d**) Proposed controller.

In the case of the PI controller, it was confirmed that the overshoot/undershoot of the speed occurred as expected, and that the speed magnitude differed as the parameters were changed.

In the case of the IP and 2-DOF controllers, it was confirmed that overshoot/undershoot by over-integration occurred as predicted in Figure 10, in the previous section. The influence of the parameter variation was also confirmed. In contrast, in the case of the proposed controller, it was confirmed that the overshoot/undershoot did not occur, and it was barely affected even when parameter fluctuation occurred.

5.2. Ramp Command Response

The test for applying the ramp command was conducted similar to the test in the previous section. The result of the test wherein the ramp command was applied while the vehicle was stationary is shown in Figures 16–18. A target command of 3000 rpm, with a command change rate of 3000 rpm/s was applied for each controller. The difference between the command speed and the feedback speed was based on 100 ms before the command reached 3000 rpm, to confirm the order followability.

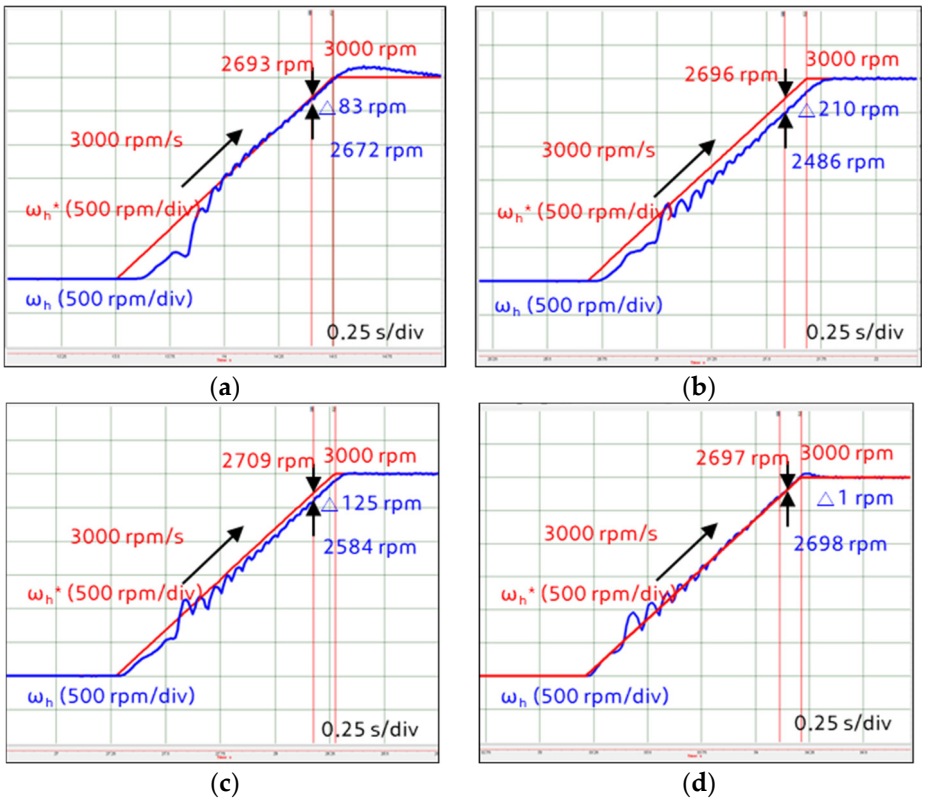

Figure 16. Speed control for ramp command (at 3000 rpm/s, parameters varied by 50%). (**a**) PI controller, (**b**) IP controller, (**c**) 2-DOF controller, and (**d**) Proposed controller.

In the case of the steady-state error, results similar to those listed in Table 6 were obtained. However, owing to the vibration component of the C2 frequency (according to the position of the engine crankshaft), it was confirmed that the magnitude difference of the HSG speed fluctuation at the time of measurement appeared at approximately 30 rpm.

5.3. Vehicle Start Response

The result of the engine clutch engagement time according to each control method when starting after stopping can be seen in Figures 19–21. To compare the performance of the controller under similar conditions, the accelerator pedal depth (APD) was maintained at 30% while the brake was applied. Subsequently, the test was conducted under the condition that the vehicle departed when the APD was

maintained and the foot was released from the brake pedal. When the APD is operated as similarly as possible between the tests, the driver's demand power is transmitted to vehicles in a similar manner in each test for each controller; therefore, similar test conditions are maintained, including the slope of the speed command and the engine start timing.

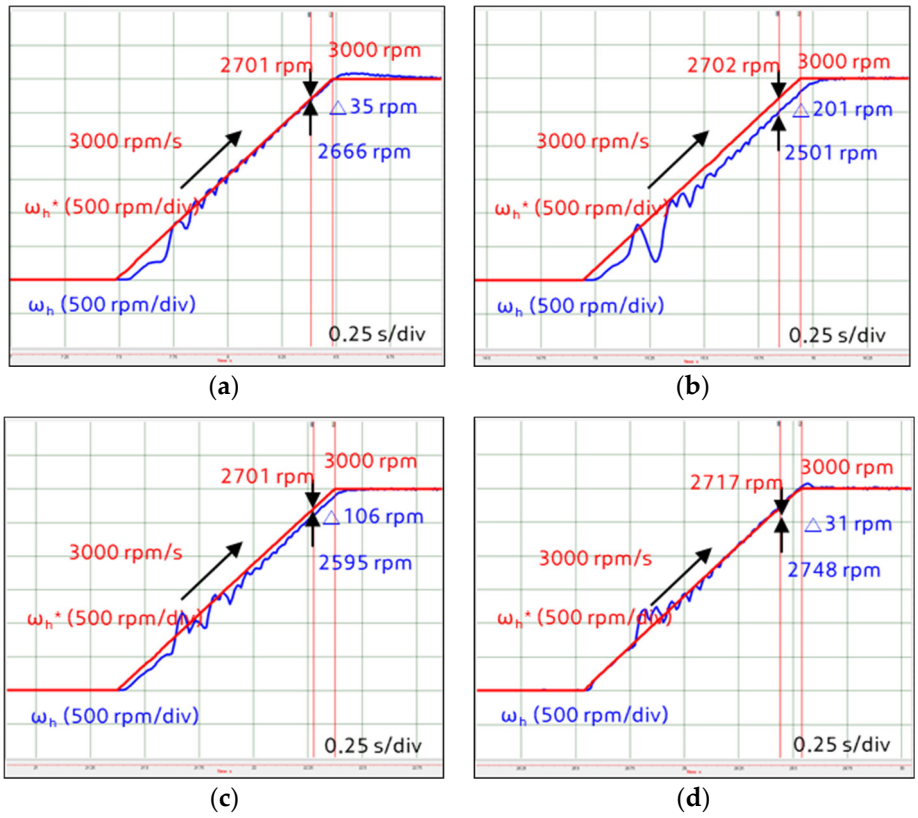

Figure 17. Speed control for ramp command (at 3000 rpm/s, parameters varied by 100%). (**a**) PI controller, (**b**) IP controller, (**c**) 2-DOF controller, and (**d**) Proposed controller.

Compared with the conventional PI controller, the proposed controller was able to reduce the engine clutch engagement time by approximately 31.5% under these conditions.

This reduction in time could reduce unnecessary energy consumed to maintain the engine's rotational speed using the HSG by reducing the EV→HEV mode changing time in a parallel hybrid vehicle with an engine clutch.

In addition, it was possible to improve EV acceleration response, which is one of the disadvantages of HEVs, by shortening the engine clutch engagement time so that the torque of the engine can be used quickly. The results of the engine clutch engagement test in a similar situation with different parameter variations for each controller structure are compared in Table 7.

Table 7. Engine clutch engagement time comparison.

	Parameters Variation	**Control Method**			
		PI	**IP**	**2-DOF**	**Proposed**
Engagement Time (ms)	50%	859	-	609	588
		Base	-	−29.1%	−31.5%
	100%	689	948	648	599
		Base	37.6%	−6.0%	−13.1%
	250%	679	1089	588	569
		Base	58.1%	−14.7%	−17.4%

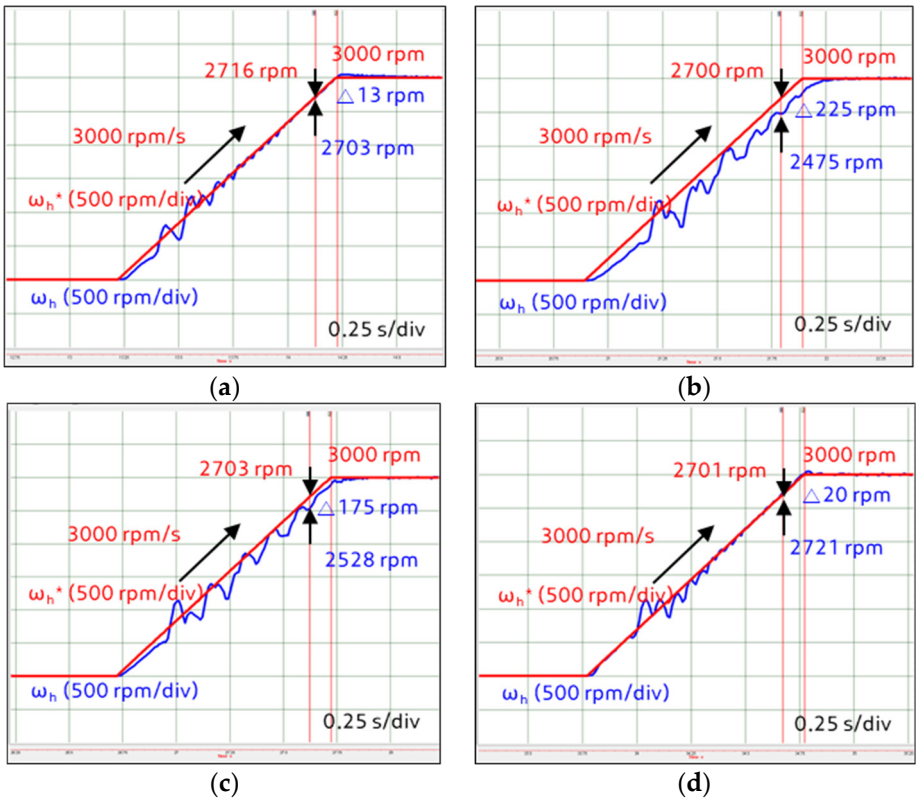

Figure 18. Speed control for ramp command (at 3000 rpm/s, parameters varied by 250%). (**a**) PI controller, (**b**) IP controller, (**c**) 2-DOF controller, (**d**) and Proposed controller.

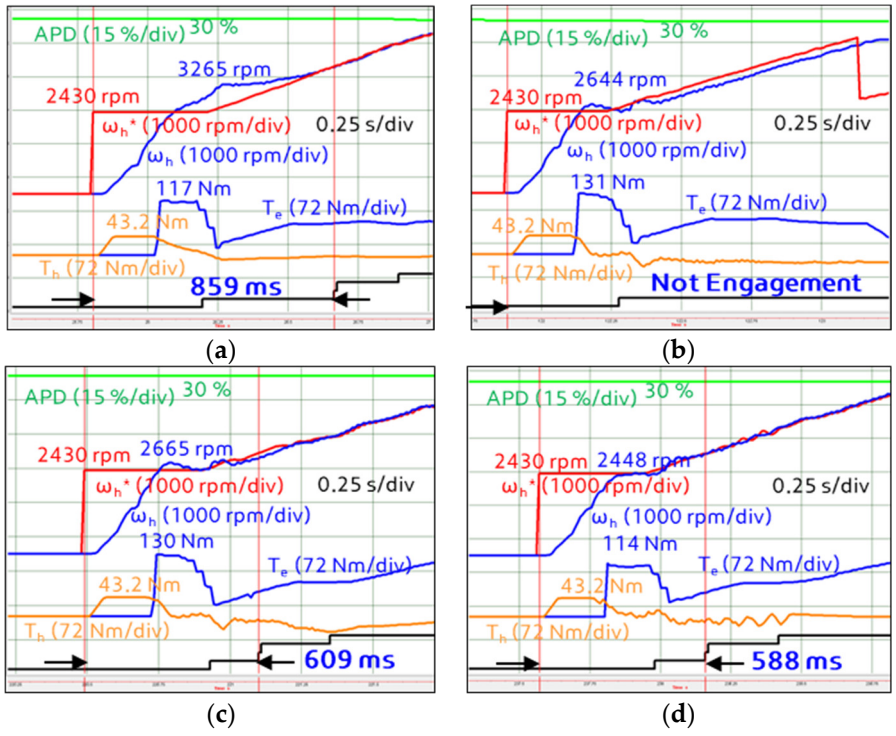

Figure 19. Speed control test result for engine clutch engagement during vehicle launching (at 30% APD, parameters varied by 50%). (**a**) PI controller, (**b**) IP controller, (**c**) 2-DOF controller, and (**d**) Proposed controller.

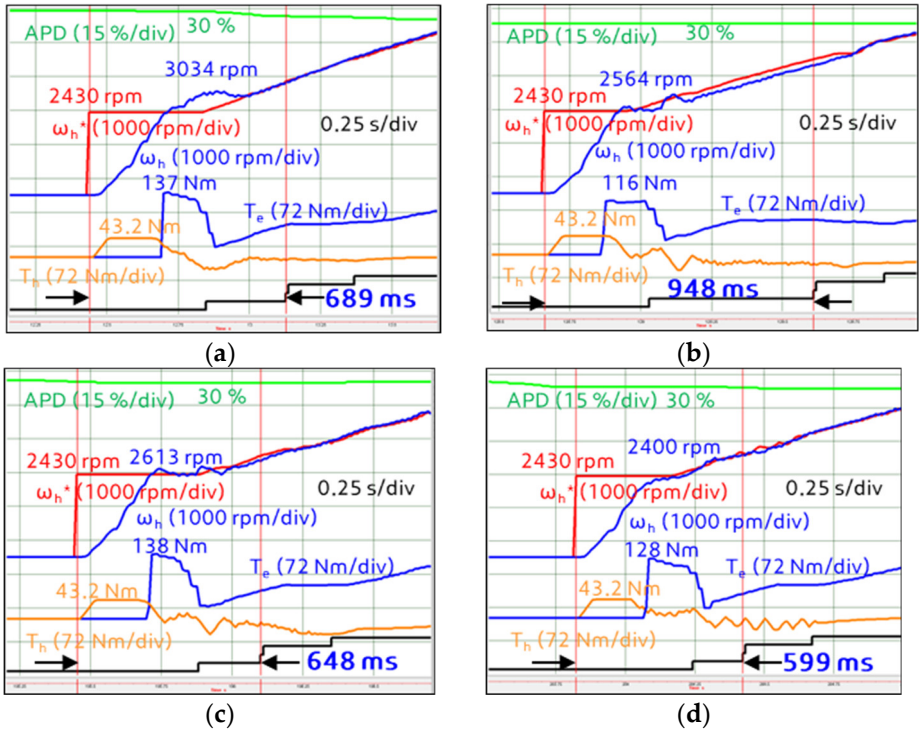

Figure 20. Speed control test result for engine clutch engagement during vehicle launching (at 30% APD, parameters varied by 100%). (**a**) PI controller, (**b**) IP controller, (**c**) 2-DOF controller, and (**d**) Proposed controller.

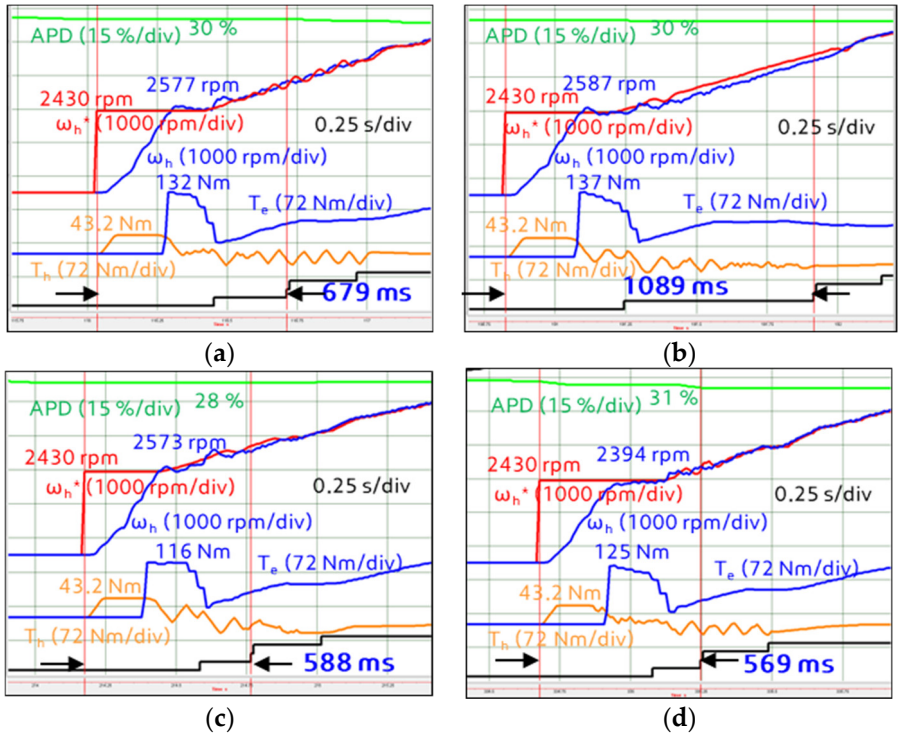

Figure 21. Speed control test result for engine clutch engagement during vehicle launching (@ 30% APD, parameters varied by 250%). (**a**) PI controller, (**b**) IP controller, (**c**) 2-DOF controller, and (**d**) Proposed controller.

6. Conclusions

This study proposes a speed control algorithm without overshoot and phase delay when the engine clutch is engaged as a method for improving the starting performance of a hybrid vehicle with a TMED system. We compared the performances of conventional controllers and the proposed controller by analyzing the system transfer function and performed simulations reflecting vehicle profiles and system constraints. In addition, the effectiveness of the proposed method was verified by confirming whether the predicted results and test results agreed with the results of the actual vehicle tests.

Based on these results, the drivability of the TMED vehicle was improved, and a foundation has been developed to shorten the development time of other types of vehicles by using a speed controller that operates as designed. However, although a speed controller could be designed as suggested for single-mass systems in this study, further research is needed on speed control of two-mass systems connected by wheels through drive motors and long drive shafts, such as in electric vehicles.

Author Contributions: Conceptualization: B.Y. and H.M.; methodology: B.Y.; software: B.Y.; validation: B.Y., K.K. and H.M.; formal analysis: K.K.; investigation: B.Y.; resources: B.Y.; data curation: K.K.; writing—original draft preparation: B.Y.; writing—review and editing: H.M.; visualization: K.K. All authors have read and agreed to the published version of the manuscript.

Funding: This research received no external funding.

Conflicts of Interest: The authors declare no conflict of interest.

References

1. LaFrance, R.C.; Schult, R.W. Electrical systems for hybrid vehicles. *IEEE Trans. Veh. Technol.* **1973**, *22*, 13–19. [CrossRef]
2. Kim, H.; Wi, J.; Yoo, J.; Son, H.; Kim, H.; Park, C. Influence of Number of Gear Step on Engine and Motor Operation Characteristics for Parallel HEV. In Proceedings of the 2018 Thirteenth International Conference on Ecological Vehicles and Renewable Energies (EVER), Monte-Carlo, Monaco, 10–12 April 2018; pp. 1–7.
3. Seung-Ki, S. *Control of Electric Machine Drive Systems; (in Korean)*; Hongrung: Seoul, Korea, 2007; pp. 240–245.
4. Nandam, P.K.; Sen, P.C. Analog and Digital Speed Control of DC Drives Using Proportional-Integral and Integral-Proportional Control Techniques. *IEEE Trans. Ind. Electron.* **1987**, *2*, 227–233. [CrossRef]
5. Umeno, T.; Hori, Y. Robust speed control of DC servomotors using modern two degrees-of-freedom controller design. *IEEE Trans. Ind. Electron.* **1991**, *38*, 363–368. [CrossRef]
6. Li, S.; Liu, Z. Adaptive Speed Control for Permanent-Magnet Synchronous Motor System with Variations of Load Inertia. *IEEE Trans. Ind. Electron.* **2009**, *56*, 3050–3059.
7. Lin, F.J.; Lee, T.S.; Lin, C.H. Robust H∞ controller design with recurrent neural network for linear synchronous motor drive. *IEEE Trans. Ind. Electron.* **2003**, *50*, 456–470.
8. Lai, C.; Shyu, K.-K. A novel motor drive design for incremental motion system via sliding-mode control method. *IEEE Trans. Ind. Electron.* **2005**, *52*, 499–507. [CrossRef]
9. Baik, I.-C.; Kim, K.-H.; Youn, M.-J. Robust nonlinear speed control of PM synchronous motor using boundary layer integral sliding mode control technique. *IEEE Trans. Control Syst. Technol.* **2000**, *8*, 47–54. [CrossRef]
10. Kim, K.-H.; Youn, M.-J. A nonlinear speed control for a PM synchronous motor using a simple disturbance estimation technique. *IEEE Trans. Ind. Electron.* **2002**, *49*, 524–535.
11. Li, S.; Liu, H.; Ding, S. A speed control for a PMSM using finite-time feedback control and disturbance compensation. *Trans. Inst. Meas. Control* **2010**, *32*, 170–187.
12. Li, C.; Chen, M.; Gao, S. Fractional Order PI Speed Control for Permanent Magnet Synchronous Motor Drives. In Proceedings of the 11th World Congress on Intelligent Control and Automation, Shenyang, China, 29 June–4 July 2014; pp. 4681–4685.
13. Liaw, C.M.; Cheng, S.Y. Fuzzy two-degrees-of-freedom speed controller for motor drives. *IEEE Trans. Ind. Electron.* **1995**, *42*, 209–216. [CrossRef]
14. Zhen, L.; Xu, L. Fuzzy learning enhanced speed control of an indirect field-oriented induction machine drive. *IEEE Trans. Control Syst. Technol.* **2000**, *8*, 270–278. [CrossRef]

15. Kung, Y.S.; Ouyang, M.; Liaw, C.M. Adaptive speed control for induction motor drives using neural networks. *IEEE Trans. Ind. Electron.* **1995**, *42*, 25–32. [CrossRef]
16. Chen, T.-C.; Sheu, T.-T. Model reference neural network controller for induction motor speed control. *IEEE Trans. Energy Convers.* **2002**, *17*, 157–163. [CrossRef]
17. Bang, J.S.; Choi, S.H.; Ko, Y.K.; Kim, T.S.; Kim, S. The Engine Clutch Engagement Control for Hybrid Electric Vehicles. In Proceedings of the 2018 IEEE Conference on Control Technology and Applications (CCTA), Copenhagen, Denmark, 21–24 August 2018; pp. 1448–1453.
18. Kim, H.-I.; Cho, W.; Lee, K. A Fundamental Study of Friction Characteristics According to the Temperature of Engine Oil (in Korean). In Proceedings of the KSAE 2007 Spring Conference, Changwon, Korea, 21–23 June 2007; pp. 69–74.
19. Kwon, T.-S.; Sul, S.-K.; Nakamura, H.; Tsuruta, K. Identification of the Mechanical Parameters for Servo Drive. In Proceedings of the Conference Record of the 2006 IEEE Industry Applications Conference Forty-First IAS Annual Meeting, Tampa, FL, USA, 8–12 October 2006; pp. 905–910.
20. Seok, J.-K.; Lee, D.-C. Speed Controller Design Based on Current Controller Dynamics for Industry Servo Applications (in Korean). In Proceedings of the KIPE Conference, Seoul, Korea, 16 November 2002; pp. 465–471.
21. Cho, Y.; Byen, B.-J.; Lee, H.-S.; Cho, K.Y. A Single-Loop Repetitive Voltage Controller with an Active Damping Control Technique. *Energies* **2017**, *10*, 673. [CrossRef]
22. Valenzuela, M.A.; Lorenz, R.D. Startup and commissioning procedures for electronically line-shafted paper machine drives. *IEEE Trans. Ind. Appl.* **2002**, *38*, 966–973. [CrossRef]